

ИСПОЛЬЗОВАНИЕ МЕХАНОХИМИЧЕСКОЙ И ПЛАЗМОХИМИЧЕСКОЙ ОБРАБОТОК ПРИ СИНТЕЗЕ КАТАЛИТИЧЕСКИХ СИСТЕМ НА ОСНОВЕ ВЕРМИКУЛИТА И ОКСИХЛОРИДА ЦИРКОНИЯ

Н.Е. Гордина, А.А. Мельников, Г.И. Гусев, А.А. Гуцин, Р.Н. Румянцев, И.А. Астраханцева

Наталья Евгеньевна Гордина (ORCID 0000-0002-1067-4688), Антон Андреевич Мельников (ORCID 0000-0003-3101-5929), Руслан Николаевич Румянцев (ORCID 0000-0002-7763-2028)

Кафедра технологии неорганических веществ, Ивановский государственный химико-технологический университет, Шереметевский проспект, 7, Иваново, Российская Федерация, 153000

E-mail: gordinane@mail.ru, melnikoffwork@yandex.ru*, rnr86@yandex.ru

Григорий Игоревич Гусев (ORCID 0000-0002-8528-3403), Андрей Андреевич Гуцин (ORCID 0000-0003-2655-1671)

Кафедра промышленной экологии, Ивановский государственный химико-технологический университет, пр. Шереметевский, 7, Иваново, Российская Федерация, 153000

E-mail: gusevisuct@gmail.com ecolog@isuct.ru

Ирина Александровна Астраханцева (ORCID: 0000-0003-2841-8639)

Кафедра информационных технологий и цифровой экономики, Ивановский государственный химико-технологический университет, Шереметевский проспект, 7, Иваново, Российская Федерация, 153000

E-mail: i.astrakhantseva@mail.ru

В работе исследованы различные подходы к синтезу каталитических систем на основе вермикулита и диоксида циркония, базирующиеся на использовании механохимической и плазмохимической обработок. Определено их влияние на структуру и свойства катализаторов для удаления токсичного 2,4-дихлорфенола из водного раствора. Процесс механохимической активации (МХА) контролируется с помощью рентгенофазового анализа, инфракрасной спектроскопии и сканирующей электронной микроскопии. Размер частиц вермикулита измерялся с помощью сканирующей электронной микроскопии и рассчитан с использованием данных рентгеновской дифракционной спектроскопии. Для характеристики степени механохимической активации были использованы размеры областей когерентного рассеивания и величина микродеформаций. Были проанализированы такие параметры, как: изменение базального расстояния, гидратационные состояния вермикулита, площадь удельной поверхности, подробно рассмотрены изотермы адсорбции-десорбции азота с поверхности образцов, построены кинетические зависимости разложения 2,4-дихлорфенола в водном растворе. В результате проделанной работы обнаружен положительный эффект от механохимической и плазмохимической обработки систем на основе вермикулита и диоксида циркония. Полученные образцы обладают развитой морфологией поверхности, при введении диоксида циркония уменьшаются области когерентного рассеивания и происходит накопление микродеформаций, что связано с внедрением Zr^{4+} в межслойные пространства вермикулита. Использование механохимической и плазмохимической обработки увеличивает как степень разложения (с 60 до 79% при заданных параметрах обработки), так и скорости, энергетические вклады в процесс деструкции, а сама вермикулитовая каталитическая система более эффективна в совмещённых плазменно-каталитических процессах (СПКП) разложения 2,4-ДХФ, чем Pt/Al₂O₃.

Ключевые слова: катализатор, вермикулит, оксихлорид циркония, механохимическая активация, плазмохимическая обработка

MECHANOCHEMICAL AND PLASMACHEMICAL PROCESSING IN THE SYNTHESIS OF CATALYTIC SYSTEMS BASED ON VERMICULITE AND ZIRCONIUM OXYCHLORIDE

N.E. Gordina, A.A. Melnikov, G.I. Gusev, A.A. Gushchin, R.N. Rumyantsev, I.A. Astrakhantseva

Natalya E. Gordina (ORCID 0000-0002-1067-4688), Anton A. Melnikov (ORCID 0000-0003-3101-5929)*, Ruslan N. Rumyantsev (ORCID 0000-0002-7763-2028)

Department of Technology of Inorganic Substances, Ivanovo State University of Chemistry and Technology, Sheremetevskiy ave., 7, Ivanovo, 153000, Russia

E-mail: gordinane@mail.ru, melnikoffwork@yandex.ru*, rnr86@yandex.ru

Grigoriy I. Gusev (ORCID 0000-0002-8528-3403), Andrey A. Gushchin (ORCID 0000-0003-2655-1671)

Department of Industrial Ecology, Ivanovo State University of Chemistry and Technology, Sheremetevskiy ave., 7, Ivanovo, 153000, Russia

E-mail: gusevisuct@gmail.com, ecolog@isuct.ru

Irina A. Astrakhantseva (ORCID 0000-0003-2841-8639)

Department of Information Technology and Digital Economy, Ivanovo State University of Chemistry and Technology, Sheremetevskiy ave., 7, Ivanovo, 153000, Russia

E-mail: i.astrakhantseva@mail.ru

Various approaches to the synthesis of catalytic systems based on vermiculite and zirconium dioxide, founded on the use of mechanochemical and plasmachemical processing, are investigated in this work. Their influence on the structure and properties of catalysts for removing toxic 2,4-dichlorophenol from an aqueous solution is determined. The activation process is controlled by X-ray diffraction, IR-spectroscopy, and scanning electron microscopy. The size of the vermiculite particle was directly measured by scanning electron microscopy and calculated using X-ray diffraction spectroscopy data. To characterize the degree of mechanochemical activation (MCA), the size of the coherent scattering region and the value of micro deformations were used. We analyzed such parameters as a change in basal distance, hydration states of vermiculite, specific surface area, kinetic dependences of the decomposition of 2,4-dichlorophenol in an aqueous solution. A positive effect of mechanochemical and plasmachemical processing of systems based on vermiculite and zirconium dioxide was found. The use of these methods increases both the degree of decomposition (from 60 to 79% at given processing parameters) and the rate, energy contributions to the destruction process; and the vermiculite catalytic system itself is more efficient in combined plasma-catalytic processes (CPCP) of decomposition of 2,4-DCP than Pt/Al₂O₃.

Key words: catalyst, vermiculite, zirconium oxychloride, mechanochemical activation, plasmachemical processing

Для цитирования:

Гордина Н.Е., Мельников А.А., Гусев Г.И., Гушчин А.А., Румянцев Р.Н., Астраханцева И.А. Использование механохимической и плазмохимической обработок при синтезе каталитических систем на основе вермикулита и оксихлорида циркония. *Изв. вузов. Химия и хим. технология.* 2022. Т. 65. Вып. 5. С. 43–57

For citation:

Gordina N.E., Melnikov A.A., Gusev G.I., Gushchin A.A., Rumyantsev R.N., Astrakhantseva I.A. Mechanochemical and plasmachemical processing in the synthesis of catalytic systems based on vermiculite and zirconium oxychloride. *Chem-ChemTech [Izv. Vyssh. Uchebn. Zaved. Khim. Khim. Tekhnol.]*. 2022. V. 65. N 5. P. 43–57

INTRODUCTION

At the moment, the efficiency of many technological processes, the selection of the optimal scheme and equipment directly depend on the properties of the catalyst used. At the same time, the determining factor

in the choice of a catalytic system is the specific requirements associated with the process conditions and the type of processed raw materials, including the possibility of the finished product molding [1-3].

However, the problems of direct synthesis of catalysts, which would allow, among other things, to predict the properties of the obtained materials, control

their properties (activity, selectivity), and also optimize the stages of functional preparation and processing of the feedstock, have not been sufficiently studied [4].

Inorganic materials of natural origin with sufficient catalytic potential include layered hydrosilicate – vermiculite; the package structure determines its specific properties. At the same time, there is a direct dependence on changes in the surface area and structure of the mineral, which is directly determined by the method of modification. By various forms of impact on vermiculite, the main structure is stratified, both into separate layers and into a set of packages of several layers, freely oriented and independent in the solvent matrix [5]. To date, there is a large amount of data in the literature on the physicochemical properties and activity of catalysts both based on zirconium oxychloride and oxides of other metals (Fe^{3+} , Y^{3+} , Al^{3+} , Mn^{3+}) [6-11]. Their strong acidic properties make it possible to use them in a variety of technological petrochemical processes (isomerization, alkylation, acylation, purification of aqueous solutions, gas emissions from organic and inorganic pollutants, etc.) [12-17]. However, most of the presented techniques for synthesizing catalytic systems require significant energy and material costs for their implementation [18]. The search for new ways of targeted synthesis of catalytic systems in addition to thermodynamically reversible routes with the production of metastable phases will contribute to solving this problem [19-20]. These include mechanochemical activation (MCA) and plasmachemical processing (PCP) [21-22]. A certain new direction in plasmachemical systems for protecting the environment, which makes it possible to significantly intensify the processes of decomposition of organic compounds and reduce energy costs, is also the use of combined plasma processes with traditional [23-25]. In combined plasma-catalytic processes (CPCP), when a model solution enters the reactor, where a catalyst is located in the discharge zone, active plasma components affect both the catalyst and the solution, which can lead to accelerated degradation of organic compounds dissolved in water, as well as to change in the composition of the resulting degradation products. Therefore, the study of the transformation kinetics of organic compounds under the action of CPCP, on the example of a dielectric barrier discharge (DBD) with a catalyst layer inside, is relevant.

Such systems can be used to destroy toxic and oxidation-resistant organic compounds that pose a severe threat to the environment and public health [26]. These substances are chlorinated phenols (CP), belonging to the group of priority organic pollutants

ubiquitous in the environment [27]. They are highly toxic, carcinogenic, and resistant to biodegradation [28-29].

One of the most toxic CP is 2,4-dichlorophenol (2,4-DCP) [30-31].

Chlorinated herbicide production, organic synthesis, landfills, incinerator plants are the sources of 2,4-DCP in the environment [32-34].

Despite the lack of direct commercial use, 2,4-DCP enters industrial wastewater at concentrations from 10 to 1000 mg/l [35]. There are various physicochemical methods for purifying emissions and wastewater from CP. However, most of them have various disadvantages, such as low degradation efficiency, high economic costs, and the formation of more toxic end products [36-37].

These methods are characterized by a high potential for creating environmentally friendly methods for purifying gas emissions and effluents from highly toxic compounds and have higher economic performance than traditional methods. Eliminating the solvent allows achieving new material characteristics or introducing a new component without an intermediate agent, thereby increasing the efficiency of the process.

Thus, the relevance of this research is the creation of new types of highly active catalytic systems based on vermiculite and zirconium oxychloride in combined plasma-catalytic processes used to purify aqueous solutions and gas emissions from organic and inorganic pollutants.

EXPERIMENTS

MATERIALS

The work investigated natural vermiculite of the Kovdor vermiculite deposit, with a grain size of up to 0.6 mm. The chemical composition of vermiculite corresponded to: SiO_2 (37.2%), Al_2O_3 (6.2%), CaO (15.3%), Fe_2O_3 (19%), MgO (13.1%)

In order to obtain the ZrO_2 , we used the commercial zirconium oxychloride octahydrate $\text{ZrOCl}_2 \cdot 8\text{H}_2\text{O}$ (CAS no. 13520-92-8).

Commercial oxygen and nitrogen were used as plasma-forming gases.

PREPARATION OF THE CATALYSTS

The synthesis of catalysts was carried out with joint mechanochemical activation of the initial components: vermiculite and zirconium oxychloride octahydrate ($\text{ZrOCl}_2 \cdot 8\text{H}_2\text{O}$), taken in a ratio that provides Zr^{4+} content in the mixture of 5 wt.%. The mechanochemical activation (MCA) was performed in the vibratory roller-ring mill VM-4 (Česká Republika). The diameter of the milling chamber was 98 mm, and the total

volume of the chamber was 0.302 l. The oscillation frequency was 930 min⁻¹, and the amplitude was 10 mm. The mixture was loaded into the mill in the amount of 50 g. The energy strength was 10,2 kW kg⁻¹. The specified energy is only the net energy that is applied from the milling bodies to the powder. This value does not include the energy losses in the various mechanical components of the mill equipment. Such an approach was proposed by Heegn [38]. This allows not to take into account the specific configuration and type of used mill apparatus and make a correct evaluation of the MCA efficiency. Thus, net energy is proportional to the energy strength and processing time in the mill [39]. The MCA time was 5-30 min.

After the MCA, the water was added to the mixture. The resulted content was stirred to obtain the homogeneous plastic paste. The optimum water content was ranged from 25 to 30 wt % and was controlled by the depth of immersion of the cone. The method for determining the optimum molding moisture is described in (1). The granules with a diameter of 3 ± 0.1 mm were molded from the paste using the piston extruder. Then, the pellets were dried at 100-110 °C. The thermal treatment of dried pellets was carried out at 650 °C for 4 h.

Plasmachemical processing of the catalyst was carried out using a DBD unit that implements a coaxial arrangement of electrodes [40]. A reactor with a coaxial arrangement of electrodes is shown in Fig. 1.

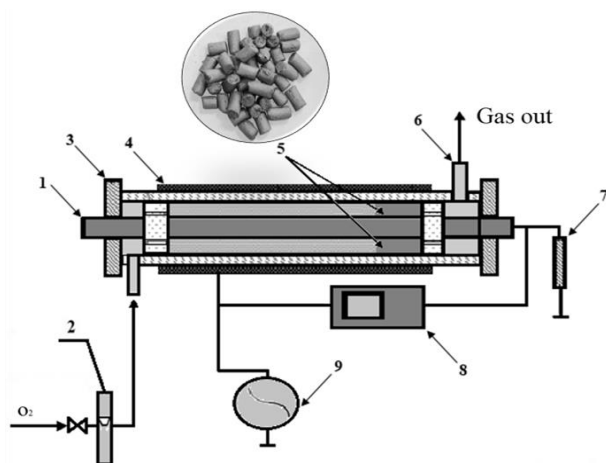


Fig. 1. Scheme of the experimental setup. 1 – inner electrode; 2 – gas cylinder with a flow rate meter; 3 – Teflon insert; 4 – external electrode; 5 – layer of the processed catalyst; 6 – gas mixture outlet; 7 – resistor 100 Ohm; 8 – digital two-channel oscilloscope GW Instek GDS-2072; 9 – power supply

Рис. 1. Схема экспериментальной установки. 1 – внутренний электрод 2 – газовый баллон с расходомером; 3 – тefлоновая вставка; 4 – внешний электрод; 5 – слой обрабатываемого катализатора; 6 – выход газовой смеси; 7 – резистор 100 Ом; 8 – цифровой двухканальный осциллограф GW Instek GDS-2072; 9 – блок питания

The glass tube acting as a dielectric was made of Pyrex glass 1 mm thick. The electrodes were made of aluminium. The catalyst inside the cell was kept in the discharge zone using perforated fluoroplastic rings.

Commercial oxygen was used as the plasma-forming gas; the gas flow rate in all experiments was 8.3 ml/s. The carrier gas flow rate was controlled using a gas flow meter. The barrier discharge was excited from a high-voltage transformer. The root-mean-square voltage in the experiments was 16.5 kV. In this case, the discharge current was 13 mA. The frequency of the voltage applied to the electrodes was 800 Hz.

The volumetric power deposited in the discharge (W , W/cm³) was 8.6 W/cm³ and was determined as the power applied to 1 cm³ of the discharge zone:

$$W = \frac{U \cdot I}{V_{d.z.}} \quad (1)$$

where I , A is the current strength in the secondary circuit, U , V is the voltage, $V_{d.z.}$, cm³ is the volume of the discharge zone, calculated by the formula:

$$V_p = S_{sect.} \cdot L_{d.z.} \quad (2)$$

where $S_{sect.}$, cm² is the sectional area of the discharge zone, $L_{d.z.}$, cm is the length of the discharge zone. The volume of the discharge zone of the DBD reactor with a coaxial arrangement of electrodes for processing in nitrogen and oxygen was 25 cm³.

In all experiments, technical oxygen or nitrogen were used as plasma-forming gases, the flow rates of which in all experiments were 500 ml/min (8.33 ml/s).

COMBINED PLASMA-CATALYTIC PROCESSES (CPCP) IN WATER TREATMENT

Experiments on the destruction of 2,4-dichlorophenol present in aqueous solutions were carried out to confirm the oxidative efficiency of the synthesized catalysts.

The scheme of the experimental setup for the treatment of aqueous solutions of 2,4-DCP in DBD is given in [41].

The contact time with the discharge zone of the reactor τ_c varied in the range of approximately 1.2-2.9 s. The values of τ_c were calculated by the formula (3):

$$\tau_c = \frac{\pi DhL}{Q} \quad (3)$$

where h is the thickness of the liquid layer at laminar flow in the gravity field can be calculated, cm²; $L = 8$ cm is the length of the discharge zone, Q is the solution flow rate, cm³/s.

The thickness of the liquid layer during laminar flow in the gravity field can be calculated [42]:

$$h = 0.908 \left(\frac{v^2}{g} \text{Re} \right)^{1/3} \quad (4)$$

where $g = 9.8 \text{ m/s}^2$ is the acceleration of gravity force, v is the kinematic viscosity (m^2/s), Re is the Reynolds criterion. The Reynolds criterion was calculated by the formula (5):

$$\text{Re} = \frac{4 \cdot Q}{\pi D v} \quad (5)$$

where Q is the volumetric flow rate of the liquid m^3/s , D is the diameter of the cylinder. Combining everything, we get (3):

$$h = \left(\frac{3v}{g} \cdot \frac{Q}{\pi D} \right)^{1/3} \quad (6)$$

The kinematic viscosity of water can be calculated by the ratio (7).

$$\nu(T) = \frac{1.78 \cdot 10^{-6}}{1 + 0.0337(T - 273) + 0.000221(T - 273)^2} \quad (7)$$

In all experiments, the mass of catalysts placed in the plasma combustion zone was 1 g. The parameters of the investigation are presented in Table 1.

Table 1

Parameters of the experiment

Таблица 1. Параметры проведения эксперимента

Parameter	Value	Unit of measurement
2,4-DCP concentration	100	mg/l
Frequency	800	Hz
The power put into the discharge	8.6	W/cm ³
Current	13	mA
Voltage	16.5	kW
Plasma gas consumption (O ₂)	0.5	l/min
Catalyst weight	1000	mg
The contact time of the solution with the plasma-catalytic zone in the reactor	1-2.9	s

The effectiveness of the purification of aqueous solutions from 2,4-DCP (α) was estimated by equation:

$$\alpha(\%) = \frac{C_0 - C}{C} \cdot 100 \quad (8)$$

where C_0 and C are the initial concentration of 2,4-DCP at the inlet to the reactor and its outlet, respectively.

The energy efficiency of the decomposition process of 2,4-DCP was estimated using the formulas for the rate and energy costs of decomposition (9) and (10):

$$W_D = K \cdot n_m \cdot \exp(-1), \quad (9)$$

$$\theta = \frac{Q \cdot C_{in} \cdot 0.63 \cdot N_{Av} \cdot 1.6 \cdot 10^{-19} \cdot 100}{P}, \quad (10)$$

where Q is the flow rate of the model solution supplied for purification, (l/s), required for the demanded degree of pollutant removal; N_{Av} is the Avogadro number,

$1.6 \cdot 10^{-19}$ is the electron charge (C), P is the power put into the discharge (W), n_{in} is the initial concentration of the substance supplied with the solution (mol/l).

TESTING PROCEDURES

In this work, the following testing procedures were used:

- The MCA was performed in the vibratory roller-milling mill VM-4 (Česká Republika). The diameter of the milling chamber was 98 mm, and the total volume of the chamber was 0.302 l. The oscillation frequency was 930 min^{-1} , and the amplitude was 10 mm. The mixture was loaded into the mill in the amount of 50 g. The MCA time was 5-30 min.
- Powder X-ray diffraction (XRD) spectroscopy. The patterns were recorded on DRON-3M X-ray diffractometer. The $\text{CuK}\alpha$ radiation ($\lambda = 0.15406 \text{ nm}$, Ni filter) was used with 40 kV and 20 mA power supply settings. The scan rate was 1 min^{-1} , and the scanning step was 0.01°.
- The scanning electron microscopy (SEM) measurements were taken with the JSM-6460 LV microscope equipped with an Energy Dispersive X-Ray Spectroscopy (EDS) and thermally assisted field emission gun operating at 5 keV.
- Fourier transformed infrared (IR) spectra of the samples were measured by Avatar 360 FT-IR ESP Spectrometer working in the wavenumber range of 4000-400 cm^{-1} with the sample prepared by KBr method, where the sample of KBr ratio was 1:100.
- N₂ adsorption-desorption isotherms were measured at 77 K on the Sorbi-MS analyzer. Samples were outgassed at 573 K before the adsorption measurements. The specific surface area was calculated from nitrogen adsorption data in the relative pressure range from 0.05 to 0.2 using the BET (Brunauer-Emmett-Teller) equation. The total pore volume was estimated from the amount of nitrogen adsorbed at a relative pressure of about 0.99.
- The content of 2,4-DCP in the samples was controlled at the inlet and outlet of the reactor using gas chromatography [43] using a Chromatec 5000.2 chromatograph (produced in Russia). The relative error of determination is 30%, with a confidence level of 0.95.

XRD CALCULATION

The interplanar spacing was derived from the diffraction equation, such as

$$d = \lambda / 2 \sin \theta, \quad (11)$$

where λ is the wavelength, d is the interplanar spacing, and θ is the diffraction angle. The crystalline phases in the XRD patterns were identified by comparing the calculated interplanar spacings with those taken from the IZA database.

Since the vermiculite type belongs to the cubic monoclinic, the lattice parameter was calculated from the equation of:

$$1/d^2 = h^2 + k^2 + l^2/a^2, \quad (12)$$

where h, k, l are the Miller indexes.

The broadening of the X-ray diffraction profile allows one to determine both the dimension of the coherent scattering region (CSR) and the value of mean-square micro deformations (MD). For this purpose, we used the modified Scherrer's equation [44]. The modified Scherrer's equation (so-called Scherrer–Selyakov equation) can be written as:

$$\beta_{ph} = \frac{\lambda}{D_{CSR} \cos \Theta} + 4\varepsilon \tan \Theta, \quad (13)$$

or, in linear form

$$\beta_{ph} \cos \Theta = \frac{\lambda}{D_{CSR}} + 4\varepsilon \tan \Theta \quad (14)$$

where β_{ph} is the physical component of the broadening, D_{CSR} is the CSR dimension, ε is the mean-square MD value, and Θ is the position of the profile centroid of the sample. The value of β_{ph} can be extracted from the total broadening profile using a Gaussian distribution as

$$\beta_s^2 = \beta_{ph}^2 + \beta_{st}^2, \quad (15)$$

where β_s is the integral half-width of the sample profile, and β_{st} is the integrated half-width of the standard sample. It was assumed that, for the standard sample (Ecolan, Russia), the measured broadening is equal to the instrumental broadening only and is associated with both device characteristics and exposure conditions.

RESULTS AND DISCUSSION

XRD AND INFRARED SPECTROSCOPY

According to the XRD data (Fig. 2-3), with an increase in the amount of energy supplied during the MCA [45] and PCP, several changes occurred in the X-ray patterns of the samples. Namely, there was a decrease in interplanar spacings under high-energy impacts on the samples, a reduction in the intensity of diffraction reflections, and their broadening after grinding. The data obtained are regular and are determined by the movement of dislocations, their emergence to the surface, and annihilation due to the elastic deformation of the crystallites of the initial components [21]. On the X-ray patterns of the original sample (Fig. 2-*a*, 3-*a*), there is the most characteristic diffraction peak for vermiculite (001) at $6.18^\circ 2\Theta$ [46-47]. At the same time, small reflexes in the region of 7.43° and 8.77° indicate the presence of some impurities of biotite and mica in vermiculite [47]. After introducing $ZrOCl_2 \cdot 5H_2O$ into the initial mixture, the intensity of

these peaks decreased significantly (Fig. 2 *c-e*, 3 *c-e*). X-ray patterns of samples *c-e* showed that the characteristic diffraction peak (001) of vermiculite was shifted to the region of $8.80^\circ 2\Theta$.

The presence of the promoting additive ZrO_2 in samples *b, c, d, e* is evidenced by reflections in the region $31-31.5^\circ 2\Theta$. The presence of zirconium in the system in the form of a zirconium oxychloride compound is evidenced by the fact that the crystallization of the oxide phase of zirconium from $ZrOCl_2 \cdot 8H_2O$ begins upon calcination from $350^\circ C$, and it proceeds in two forms: stable monoclinic (*M*) and metastable tetragonal (*T*) [12, 48, 49]. In terms of catalysis, the second *T*-form is preferred. The formation of this particular form can be explained by the fact that the metal cations contained in vermiculite act as promoters, delaying the growth of crystallites and stabilizing the nanostructured state of the oxide. This fact correlates well with literature data [12, 48, 49]. In addition, this can be associated with the formation of solid solutions of promoter cations in the ZrO_2 lattice [50-51]. The change in the basal distance in the samples in the presence of zirconium is associated with incorporating ZrO_2 into the interlayer spaces of vermiculite [47].

A clearer picture of the changes that occur during the modification of vermiculite is shown in Fig. 2, which displays a sequence of d002 intensity profiles. It should be taken into account that the interplanar spacing in vermiculite indirectly characterizes the amount of interpacket water that the mineral is able to absorb [52]. According to [53], vermiculite exists in three types of hydration states: zero (anhydrous), one- or two-layer.

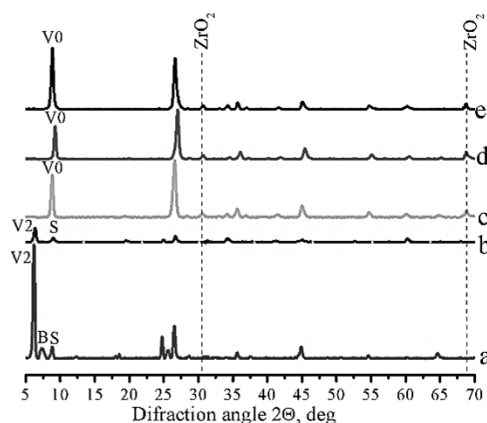


Fig. 2. XRD sample: a – initial vermiculite, b – MCA+650 °C, c – MCA+Zr5%+PCP(N₂), d – MCA+Zr5%+PCP(O₂), e – MCA+Zr5%+PCP(2x O₂). Induced phases: V₂– two-layer hydration state, V₀– zero hydration state (anhydrous), B– biotite, S– mica

Рис. 2. РФА образцов: а – исходный вермикулит, б – МХА + 650 °С, в – МХА+Zr5%+ПХО(N₂), д – МХА+Zr5%+ПХО(O₂), е – МХА+Zr5%+ПХО(2х O₂). Induced phases: V₂– двухслойное гидратное состояние, V₀–нулевое гидратное состояние (безводное), В– биотит, S– слюда

Due to MCA and PCP in the energy supply process, a change in the amount of water in the inter-layer space of the hydrated vermiculite layers was observed. The calculated values of the interplanar distances of the original and modified samples showed that the most considerable value of the interplanar distance, and, consequently, the most significant number of water layers, is characteristic of the initial vermiculite – sample *a* (14,55 Å). MCA (sample *b*) contributed to lowering of this indicator to 14.19 Å due to a decrease in the intensity of the peak in the region of $6.18^\circ 2\theta$, and its shift to high-angle regions of $6.35^\circ 2\theta$. Whereas the additional PCP (samples *d*, *c*, *e*) led to the ordering of the vermiculite structure and its dehydration. The values of interplanar spacings, depending on the PCP medium (O_2 – sample *d* and N_2 – sample *c*) and its frequency (double treatment – sample *e*), are close and are in the range of 9.66–9.95 Å.

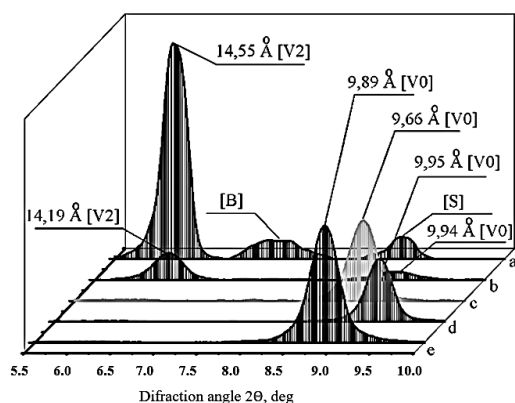


Fig. 3. XRD sample: a – initial vermiculite, b – MCA+650 °C, c – MCA+Zr5%+ PCP(N_2), d – MCA+Zr5%+ PCP(O_2), e – MCA+Zr5%+ PCP(2x O_2). Induced phases: V₂– two-layer hydration state, V₀– zero hydration state (anhydrous), B– biotite, S– mica
Рис. 3. РФА образцов: а – исходный вермикулит, б – МХА +650 °С, с – МХА+Zr5%+ПХО(N_2), д – МХА+Zr5%+ПХО(O_2), е – МХА+Zr5%+ПХО(2x O_2). Induced phases: V₂– двухслойное гидратное состояние (безводное), V₀– нулевое гидратное состояние (безводное), В– биотит, S– слюда

Based on the XRD data, the calculated values of changes in coherent scattering regions (CSR) and micro deformations (MD) (Table 2) under various methods of action on vermiculite.

Hence it follows that with an increase in the supplied energy, the calculated CSR values tended to decrease; if D_{circle} of the initial vermiculite was 260 nm, then the one of the activated samples was from 192 to 187 nm. This fact is explained by the displacement and rearrangement of vacancies for OH groups in the mineral, shown earlier in Fig. 2 and 3. There, a decrease in the intensity of reflections, their shift or disappearance, confirms the fact of a reduction in the size of crystallites in activated samples, an increase in the

level of defectiveness and structural disorder of the crystal lattice (Table 2).

Table 2

Characteristics of the microstructure of the crystal lattice of modified samples: a – initial vermiculite, b – MCA +650 °C, c – MCA+Zr5%+ PCP(N_2), d – MCA+Zr5%+ PCP(O_2), e – MCA+Zr5%+ PCP(2x O_2)

Таблица 2. Characteristics of the microstructure of the crystal lattice of modified samples: a – исходный вермикулит, б – МХА +650 °С, с – МХА+Zr5%+ПХО(N_2), д – МХА+Zr5%+ПХО(O_2), е – МХА+Zr5%+ПХО(2x O_2)

Title	CSR ¹ , nm	MD ² , %
a	260±5.2	0.41±0.01
b	192±3.84	0.72±0.01
c	187±3.74	0.63±0.01
d	194±3.88	0.65±0.01
e	197±3.94	0.75±0.02

¹CSR – coherent scattering region, nm; ²MD – micro deformations, %

¹CSR – область когерентного рассеяния, нм; ²MD – микродеформации, %

Due to the dispersion and accumulation of defects in the crystal lattice after MCA, the promoting additive led to a decrease in the unit cell volume associated with incorporating zirconium atoms and their distribution in the vermiculite crystal lattice. At the same time, the subsequent PCP is connected only with ongoing processes of plastic deformation of the crystal lattice without a significant change in the volume of the unit cell.

The data obtained by XPD are in good agreement with the results of IR spectroscopy. It was established (Fig. 4) that no new functional groups were formed in the vermiculite samples during the PCP, which is associated with the presence of the same functional groups in the structure of the studied minerals. In the IR spectrum of all samples, absorption bands were found corresponding to a layered hydrosilicate containing hydroxyl groups and a significant amount of structurally bound water. A slight reduction in the intensity of the absorption bands at 1640 cm^{-1} and 3700 cm^{-1} , representing scissoring deformation $\delta_s OH$ and symmetric stretching $\nu_s OH$ vibrations, respectively, is associated with the presence of H_2O with different degrees of bonding, as well as a decrease in the number of hydroxyl functional groups in modification process [54]. On the IR spectra of all modified vermiculites, the absorption wave at $590\text{--}620\text{ cm}^{-1}$ refers to the deformation vibrations of Si–O–M (octahedral cation), where M = Mg, Al, Fe, etc. The absorption bands at 680 cm^{-1} are due to Al–O–Si stretching vibrations, while the band at 1160 cm^{-1} is the Si–O stretching vibration in the silicon framework [55]. The *c-e* band

present on the samples in the region of 495 cm^{-1} was identified as a Zr–O bending vibration [56].

The crucial role in sorption and catalytic phenomena is played by structural defects, including acid-base centers of various nature on the sample surface. Analysis of the results of the IR spectra study showed that in all modified samples, the characteristic frequencies slightly changed, which is mainly caused by the interaction of water molecules, oxygen-containing fragments of silicon, aluminum, iron, magnesium, calcium, which are part of vermiculite, and as a result, changes the number of hydrated layers of vermiculite in the interlayer space.

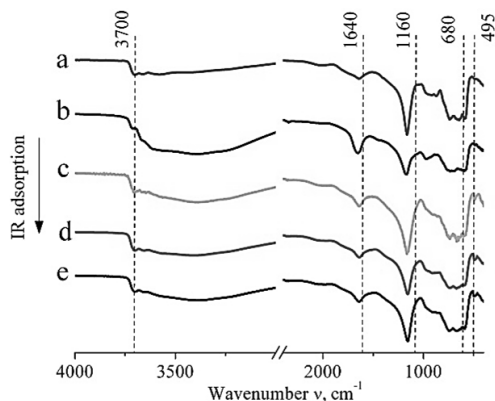


Fig. 4. IR-spectra samples: a – initial vermiculite, b – MCA +650 °C, c – MCA+Zr5%+PCP(N₂), d – MCA+Zr5%+ PCP(O₂), e – MCA+Zr5%+ PCP (2x O₂)

Рис. 4. ИК-спектры samples: a – исходный вермикулит, b – MCA +650 °C, c – MCA+Zr5%+ПХО(N₂), d – MCA+Zr5%+ПХО(O₂), e – MCA+Zr5%+ПХО(2x O₂)

MICROSTRUCTURAL ANALYSIS

Structural studies have shown that the morphology of vermiculite samples during their MCA

changes significantly (Fig. 5 b). After mechanical energy was applied, dispersion and aggregation of the samples were observed. The surface of the original vermiculite has a layered structure in the form of aggregates of flaky and petal shape, tightly adhering to each other and forming a single frame with numerous macropores that act as transport channels during heterogeneous processes. However, if particles 1 to 2 μm in size predominated in the original sample and a larger phase of 10-20 μm , then after 10 min of MCA, the crystals were agglomerated into intergrowths with an irregular arrangement of particles, forming agglomerates from 2 to 5 μm . With a decrease in the scale length of the scan, the globular structure of individual surface areas with fragments of crystalline inclusions appears. When introducing 5 wt. % zirconium into the original system (Fig. 4 c-e), the fact of agglomeration of vermiculite particles in the presence of additives was recorded; agglomerates represent the structure of “sandwich” layers. The change in the structure of vermiculite during the modification with the formation of delaminated sheets suggests that vermiculite particles are agglomeration centers from which new formations grow, in particular, for example, other functional hydroxyl groups [M - OH (M = Zr, Si, Mg, etc.) [57]. During double PCP (Fig. 5 e), the agglomeration and sticking of particles were recorded. The average dispersion is in the range of 5-10 microns; with PCP, the mineral is transformed into a denser matrix structure characterized by an almost continuous undirected mass, although the lamellar structure is visible. In the case of PCP in a medium in N₂ and O₂ (Fig. 5 c, d), vermiculite crystals have a more pronounced lamellar shape; the average dispersion is in the range of 2–20 μm , where agglomerates 10–20 μm in size are often found.

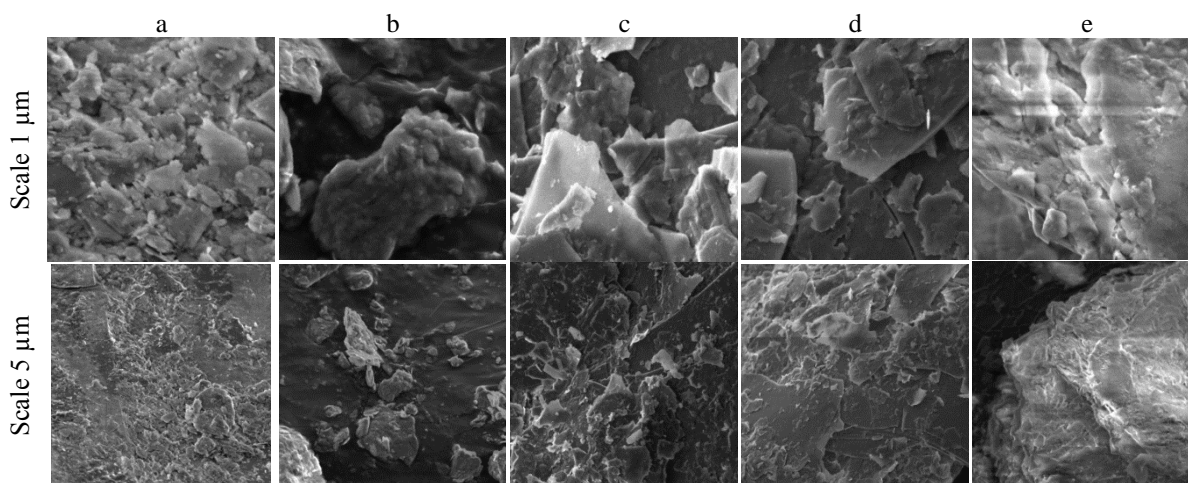


Fig. 5. SEM images samples: a – initial vermiculite, b – MCA +650 °C, c – MCA+Zr5%+ PCP(N₂), d – MCA+Zr5%+ PCP (O₂), e – MCA+Zr5%+ PCP(2x O₂)

Рис. 5. СЭМ изображения образцов: a – исходный вермикулит, b – MCA +650 °C, c – MCA+Zr5%+ПХО(N₂), d – MCA+Zr5%+ПХО(O₂), e – MCA+Zr5%+ПХО(2x O₂)

BET ANALYSIS

All obtained isotherms are of type IV and have a hysteresis loop reflecting the process of capillary condensation in mesopores. This type of isotherm is scarce in practice and is observed when nitrogen is adsorbed on some types of activated carbon. The stepped isotherms presented reflect the layer-by-layer filling of the surface with adsorbate molecules [58].

The initial vermiculite has the lowest specific surface area; it is about 7 m²/g; after MCA and heat treatment, it increases to 21,3 m²/g. There is a significant increase in the macroporous structure by more than 150% and amounts to 0,043 cm³/g, an increase in the hysteresis loop is observed, and the phenomenon of capillary condensation occurs. With the subsequent introduction of zirconium and PCP, the samples treated in N₂, O₂, and double PCP undergo significant changes: among them, the sample treated in O₂ has the largest specific surface area, it is about 15,1 m²/g, which is more than the samples treated in N₂ and double PCP, respectively. A similar correlation is observed in terms of total pore volume, where a sample of vermiculite treated in O₂ has the highest value of 0,023 cm³/g. In all samples, the hysteresis loop area broadens; however, the smallest pore diameter (up to 20 nm) is characteristic of the sample treated in N₂ and the maximum content of pores with a diameter of 5 to 7 nm reaches about 35%. In the case of sample treatment in O₂, the pore diameter increases and reaches up to 40 nm, while the maximum percentage value does not change and remains the same as for the sample treated in N₂. In the case of double PCP, the macroporous structure increases, but mesopores also occur.

The measurement of specific surface area, pore volume, and average pore size by the BET method is given in Table 3. It is shown that the formed porous structure of the original and modified samples has a specific surface ranging from 7-21.3 m²/g, with the minimum typical for the initial vermiculite (sample *a*) and the maximum for the sample obtained during 10 min of MCA and subsequent calcination at 650 °C (sample *b*).

Indeed, the initial vermiculite has most of the pores related to mesopores. However, larger mica packets have very fine macropores. Under MCA and heat treatment, the number of macropores significantly decreases, and the content of micropores and mesopores increases. It should be noted that the MCA + Zr5% + PCP(N₂) sample has the highest range of micro- and mesopores. Mesoporous materials are of great practical interest as sorbents and carriers for catalysts.

In all cases of modification, the use of PCP after MCA led to a decrease in the specific surface area

of the samples, which may be associated with burnout and sintering of the catalyst surface that occur at high temperatures formed in the discharge zone at high voltage [59-60]. In this case, the surface layers are cooled due to heat absorption in endothermic reactions on the sample surface and in the surface pores (with micropores and mesopores burning out).

Table 3

Structure characteristics of samples: a – initial vermiculite, b – MCA+650 °C, c – MCA+Zr5%+ PCP (N₂), d – MCA+Zr5%+ PCP (O₂), e – MCA+Zr5%+ PCP (2x O₂)

Таблица 3. Характеристики структуры samples: a – исходный вермикулит, b – МХА +650 °С, c – МХА+Zr5%+ПХО(N₂), d – МХА+Zr5%+ПХО(O₂), e – МХА+Zr5%+ПХО(2x O₂)

Sample name	Specific surface area S _{sp} m ² /g	Pore volume (cm ³ /g)
a	7.0±0.35	0.017±0.001
b	21.3±1.07	0.043±0.001
c	12.4±0.62	0.019±0.001
d	15.1±0.76	0.023±0.001
e	14.9±0.75	0.021±0.001

The diameter of the globules varies in the range of ~ 40-200 nm; the pores formed between the globules have a width from 4-6 nm to 13-15 nm (micropores), and the diameter of the pores formed due to the mineral structure imperfection is from 30 to 80-100 nm (mesopores). Mesopores and macropores are transport channels that provide the supply of reactant molecules to the active centers of the system and the removal of transformation products. The available micropores provide a "sieve effect", which consists in the selective sorption of only those molecules whose dimensions are less or equal to the dimensions of the micropores.

Conclusions about the surface area, the adsorbed object porosity, and the nature of the interaction between the adsorbent and adsorbate can be drawn from the isotherms. The obtained isotherm for the initial vermiculite, MCA 10 min + 650 °C, and vermiculite + two treatments DBD corresponds to the type V isotherm (according to the classification of Brunauer, Deming, Deming and Teller [58]), all subsequent modifications of vermiculite slightly change the type of isotherm and the hysteresis loop. It should be noted that PCP in N₂ and O₂ media significantly changes the hysteresis loop to increase its area and the type of the isotherm. The isotherms obtained in these cases belong to type VI – stepped isotherms; they are relatively rare and therefore are of particular theoretical interest. Indeed, the distribution of pores relative to the volume changes significantly under PCP (Fig. 6).

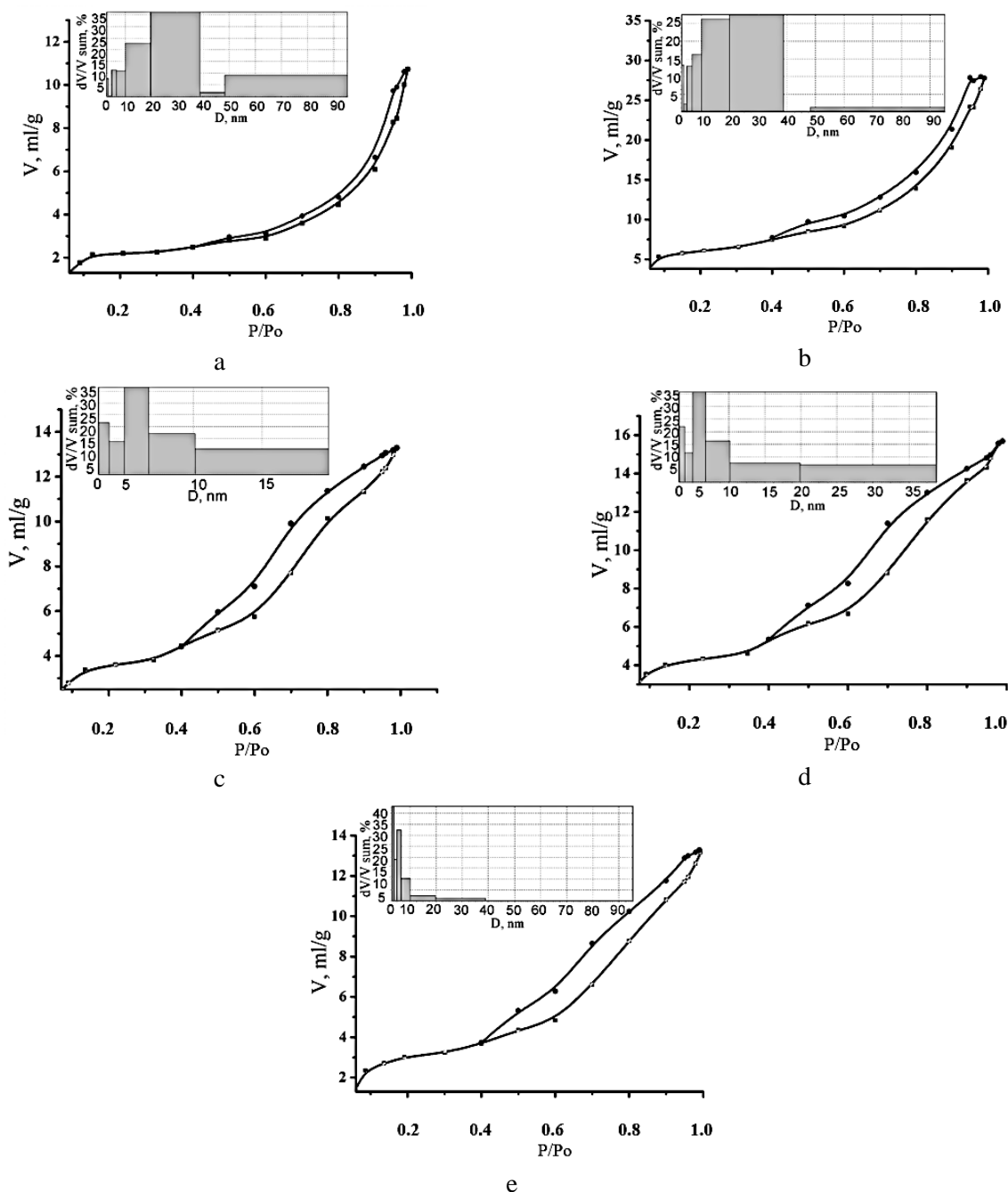


Fig. 6. Nitrogen adsorption–desorption isotherms and BJH pore size distribution curves on samples: a – initial vermiculite, b – MCA +650 °C, c – MCA+Zr5%+ PCP(N₂), d – MCA+Zr5%+ PCP(O₂), e – MCA+Zr5%+ PCP(2x O₂)

Рис. 6. Изотермы адсорбции-десорбции азота и распределение пор по размерам по методу БЭТ: а – исходный вермикулит, б – МХА +650 °С, с – МХА+Zr5%+ПХО(N₂), d – МХА+Zr5%+ПХО(O₂), e – МХА+Zr5%+ПХО(2x O₂)

RESULTS OF 2,4-DCP DESTRUCTION

The newly synthesized catalyst (vermiculite + Zr 5%) effectively destroys organic pollutants present in wastewater, which is confirmed by the results of studies of the destruction of 2,4-DCP. The kinetics and efficiency of the degradation of the test compound are shown in Fig 7. Kinetic curves of 2,4-DCP decom-

position are satisfactorily described by pseudo-first-order equations with effective rate constants (0.36 ± 0.04) and $(0.51 \pm 0.03) \text{ s}^{-1}$ when processing model solutions without a catalyst and with vermiculite + Zr 5%, respectively.

The rates of the decomposition process were $11.64 \cdot 10^{17}$ and $8.16 \cdot 10^{17} \text{ cm}^{-3} \text{ s}^{-1}$ during the treatment of model solutions with and without a catalyst in the discharge zone, respectively, and the energy costs were

0.017 and 0.012 molecules/100 eV. Thus, the use of vermiculite + Zr 5% increases both the degree of decomposition (from 60 to 79% at the given processing parameters) and the speed and energy contributions to the degradation process, and the catalyst itself is more efficient in combined plasma-catalytic processes (CPCP) for the decomposition of 2,4-DCP than Pt/Al₂O₃ (41).

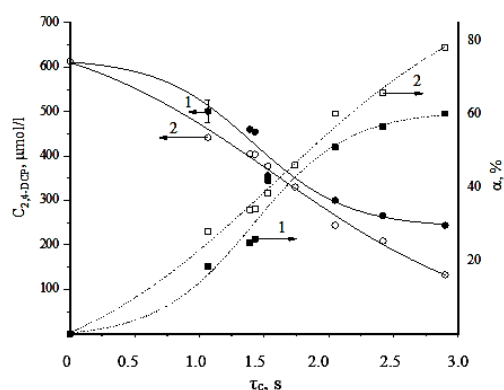


Fig. 7. Change of the 2,4-DCP concentration depending on the time of treatment in DBD (1 – without a catalyst, 2 – in the presence of vermiculite + Zr 5%)

Рис. 7. Изменение концентрации 2,4-ДХФ от времени обработки в ДБР (1 – без катализатора, 2 – в присутствии вермикулита+Zr 5%)

The destruction efficiency is supported by the fact that during the aqueous solution treatment in CPCP, an increase in the degree of mineralization of the initial compound is observed, which is 80% at the maximum (that is 1.3 times higher than during treatment in DBD). This is confirmed by both a decrease in the content of total organic carbon in the system after treatment and an increase in the concentration of carbon dioxide and carbon monoxide in the gas phase at the outlet of the reactor.

CONCLUSION

ЛИТЕРАТУРА

1. **Гордина Н.Е., Прокофьев В.Ю., Ильин А.П.** Экструзионное формование сорбентов на основе синтезированного цеолита. *Керамика и стекло*. 2005. № 62. С. 282-286. DOI: 10.1007/s10717-005-0092-3.
2. **Ильин А.А., Румянцев Р.Н., Жуков А.Б., Ильин А.П.** Механохимический синтез железо-молибденового катализатора для синтеза формальдегида. *Российские нанотехнологии*. 2016. № 11. С. 569-578. DOI: 10.1134/S1995078016050086.
3. **Прозоров Д.А., Афинеевский А.В., Смирнов Д.В., Никитин К.А.** Адсорбционная деформация при жидкофазном гидрировании кратной углеродной связи на массивном и нанесенных никелевых катализаторах. *Изв. вузов. Химия и хим. технология*. 2022. Т. 65. Вып. 1. С. 66-75. DOI: 10.6060/ivkkt.20226501.6426.

In the present work, a comparative analysis of the effect of PCP on modified vermiculite was carried out by the MCA with a promoting additive in a medium of various gases. As a result of the synthesis, more reactive samples with a developed surface morphology are formed. After introducing ZrOCl₂·8H₂O into the system, there was a downward change in the areas of coherent scattering (up to 187 nm compared to the initial vermiculite – 260 nm), an increase in micro deformations in the samples (up to 0.75% compared to the initial vermiculite 0.41%), which is associated with the incorporation of Zr⁴⁺ into the interlayer spaces of vermiculite. The use of a catalyst (vermiculite + Zr 5%) in water purification systems employing dielectric barrier discharge leads to a 20% increase in the efficiency of destruction of the 2,4-DCP present in aqueous solutions.

ACKNOWLEDGEMENTS

This work was funded by the Ministry of Science and Higher Education of the Russian Federation (Project No. FZZW-2020-0010).

The study was carried out using the resources of the Center for Shared Use of Scientific Equipment of the ISUCT (with the support of the Ministry of Science and Higher Education of Russia, grant No. 075-15-2021-671).

The authors declare the absence a conflict of interest warranting disclosure in this article.

Работа выполнена при финансовой поддержке Министерства науки и высшего образования Российской Федерации (проект № FZZW-2020-0010). Исследование выполнено с использованием ресурсов Центра коллективного пользования научной аппаратурой ИГХТУ (при поддержке Минобрнауки России, грант № 075-15-2021-671).

Авторы заявляют об отсутствии конфликта интересов, требующего раскрытия в данной статье.

REFERENCES

1. **Gordina N.E., Prokof'ev V.Y., Il'in A.P.** Extrusion Molding of Sorbents Based on Synthesized Zeolite. *Keramika i Stekol*. 2005. 62. P. 282-286 (in Russian). DOI: 10.1007/s10717-005-0092-3.
2. **Ilyin A.A., Romyantsev R.N., Zhukov A.B., Ilyin A.P.** Mechanochemical synthesis of iron-molybdenum catalyst for formaldehyde synthesis. *Russ. Nanotekhnol.*. 2016. 11. P. 569-578 (in Russian). DOI: 10.1134/S1995078016050086.
3. **Prozorov D.A., Afineevskii A.V., Smirnov D.V., Nikitin K.A.** Adsorption deformation during liquid-phase hydrogenation of unsaturated carbon bonds over bulk and supported nickel catalysts. *ChemChemTech [Izv. Vyssh. Uchebn. Zaved. Khim. Khim. Tekhnol.]*. 2022. V. 65. N 1. P. 66-75 (in Russian). DOI: 10.6060/ivkkt.20226501.6426.

4. **Чижевский А.А., Абдуллин И.Ш., Желтухин В.С.** Получение катализаторов плазменной модификацией или обработкой носителя. *Вестн. Казан. технол. ун-та*. 2015. Вып. 18. С. 159-162.
5. **Bergaya, F., Jaber, M., Lambert, J.-F.** Clays and Clay Minerals: Science, Technology and Applications. In: *Rubber-Clay Nanocomposites*. Ed. by M. Galimberti. John Wiley & Sons, Inc. 2011. P. 1-44. DOI: 10.1002/9781118092866.ch1.
6. **Aboul-Gheit A.K., El-Desouki D.S., Abdel-Hamid S.M., Ghoneim S.A., Ibrahim A.H., Gad F.K.** Sulfated Zirconia Catalysts for Low Temperature Isomerization of n-Pentane. *Egypt J. Chem.* 2012. V. 55. P. 509-527. DOI: 10.21608/ejchem.2012.1171.
7. **Bocanegra-Bernal M.H., de la Torre S.D.** Phase transitions in zirconium dioxide and related materials for high performance engineering ceramics. *J. Mater. Sci.* 2002. V 37. P. 4947-4971. DOI: 10.1023/A:1021099308957.
8. **Debsikdar J.C., Sowemimo O.S.** Effect of zirconia addition on crystallinity, hardness, and microstructure of gel-derived barium aluminosilicate, BaAl₂Si₂O₈. *J. Mater. Sci.* 1992. V. 27. P. 5320-5324. DOI: 10.1007/BF02403837.
9. **Ke X., Baki V.A.** Assessing the suitability of alkali-activated metakaolin geopolymer for thermochemical heat storage. *Micropor. Mesopor. Mater.* 2021. P. 325. DOI: 10.1016/j.micromeso.2021.111329.
10. **Valášková M., Tokarský J., Hundáková M., Zdrávková J., Smetana B.** Role of vermiculite and zirconium-vermiculite on the formation of zircon-cordierite nanocomposites. *Appl. Clay Sci.* 2013. V. 75-76. P. 100-108. DOI: 10.1016/j.clay.2013.02.015.
11. **Zou Y., Zhang R., Wang L., Xue K., Chen J.** Strong adsorption of phosphate from aqueous solution by zirconium-loaded Ca-montmorillonite. *Appl. Clay Sci.* 2020. P. 192. DOI: 10.1016/j.clay.2020.105638.
12. **Кузнецов П.Н., Твердохлебов В.П., Кузнецова Л.И., Казбанова А.В., Мельчаков Д.А., Довженко Н.Н.** Новые катализаторы на основе диоксида циркония для изомеризации алканов нефтяных фракций. *Журн. Сибир. фед. ун-та. Техника и технологии*. 2011. Вып. 4. С. 438-452.
13. **Liu R., Song H., Li B., Li X., Zhu T.** Simultaneous removal of toluene and styrene by non-thermal plasma-catalysis: Effect of VOCs interaction and system configuration. *Chemosphere*. 2021. P. 263. DOI: 10.1016/j.chemosphere.2020.127893.
14. **Mizuno A.** Generation of non-thermal plasma combined with catalysts and their application in environmental technology. *Catal. Today*. 2013. V. 211. P. 2-8. DOI: 10.1016/j.cattod.2013.03.029.
15. **Thevenet F., Sivachandiran L., Guaitella O., Barakat C., Rousseau A.** Plasma-catalyst coupling for volatile organic compound removal and indoor air treatment: a review. *J. Phys. D: Appl. Phys.* 2014. V. 47. DOI: 10.1088/0022-3727/47/22/224011.
16. **Tu X., Christopher Whitehead J., Nozaki T.** Plasma Catalysis. Switzerland. Springer, Cham. 2019. DOI: 10.1007/978-3-030-05189-1.
17. **Van Durme J., Dewulf J., Leys C., Van Langenhove H.** Combining non-thermal plasma with heterogeneous catalysis in waste gas treatment: A review. *Appl. Catal.* 2008. V. 78. P. 324-333. DOI: 10.1016/j.apcatb.2007.09.035.
18. **Пармон В.Н., Носков А.С., Анфимова Н.П., Шмачкова В.П.** Состояние и перспективы развития каталитической подотрасли и разработок по катализу в России. *Катализ в пром-ти*. 2016. Вып. 1. С. 6-20.
19. **Gordina N.E., Prokof'ev V.Y., Hmylova O.E., Kul'pina Y.N.** Effect of ultrasound on the thermal behavior of the mixtures for the LTA zeolite synthesis based on metakaolin. *J. Therm. Anal.* 2017. V. 129. P. 1415-1427. DOI: 10.1007/s10973-017-6357-6.
4. **Chizhevskij A.A., Abdullin I.Sh., Zheltukhin V.S.** Preparation of catalysts by plasma modification or carrier treatment. *Vestn. Kazan. Tekhnol. Un-ta*. 2015. 18. P. 159-162 (in Russian).
5. **Bergaya, F., Jaber, M., Lambert, J.-F.** Clays and Clay Minerals: Science, Technology and Applications. In: *Rubber-Clay Nanocomposites*. Ed. by M. Galimberti. John Wiley & Sons, Inc. 2011. P. 1-44. DOI: 10.1002/9781118092866.ch1.
6. **Aboul-Gheit A.K., El-Desouki D.S., Abdel-Hamid S.M., Ghoneim S.A., Ibrahim A.H., Gad F.K.** Sulfated Zirconia Catalysts for Low Temperature Isomerization of n-Pentane. *Egypt J. Chem.* 2012. V. 55. P. 509-527. DOI: 10.21608/ejchem.2012.1171.
7. **Bocanegra-Bernal M.H., de la Torre S.D.** Phase transitions in zirconium dioxide and related materials for high performance engineering ceramics. *J. Mater. Sci.* 2002. V 37. P. 4947-4971. DOI: 10.1023/A:1021099308957.
8. **Debsikdar J.C., Sowemimo O.S.** Effect of zirconia addition on crystallinity, hardness, and microstructure of gel-derived barium aluminosilicate, BaAl₂Si₂O₈. *J. Mater. Sci.* 1992. V. 27. P. 5320-5324. DOI: 10.1007/BF02403837.
9. **Ke X., Baki V.A.** Assessing the suitability of alkali-activated metakaolin geopolymer for thermochemical heat storage. *Micropor. Mesopor. Mater.* 2021. P. 325. DOI: 10.1016/j.micromeso.2021.111329.
10. **Valášková M., Tokarský J., Hundáková M., Zdrávková J., Smetana B.** Role of vermiculite and zirconium-vermiculite on the formation of zircon-cordierite nanocomposites. *Appl. Clay Sci.* 2013. V. 75-76. P. 100-108. DOI: 10.1016/j.clay.2013.02.015.
11. **Zou Y., Zhang R., Wang L., Xue K., Chen J.** Strong adsorption of phosphate from aqueous solution by zirconium-loaded Ca-montmorillonite. *Appl. Clay Sci.* 2020. P. 192. DOI: 10.1016/j.clay.2020.105638.
12. **Kuznetsov P.N., Tverdokhlebov V.P., Kuznetsova L.I., Kazbanova A.V., Mel'chakov D.A., Dovzhenko N.N.** New catalysts based on zirconium dioxide for the isomerization of alkanes of petroleum fractions. *Zhurn. Sibir. Fed. Un-ta. Tekhnika Tekhnol.* 2011. 4. P. 438-452 (in Russian).
13. **Liu R., Song H., Li B., Li X., Zhu T.** Simultaneous removal of toluene and styrene by non-thermal plasma-catalysis: Effect of VOCs interaction and system configuration. *Chemosphere*. 2021. P. 263. DOI: 10.1016/j.chemosphere.2020.127893.
14. **Mizuno A.** Generation of non-thermal plasma combined with catalysts and their application in environmental technology. *Catal. Today*. 2013. V. 211. P. 2-8. DOI: 10.1016/j.cattod.2013.03.029.
15. **Thevenet F., Sivachandiran L., Guaitella O., Barakat C., Rousseau A.** Plasma-catalyst coupling for volatile organic compound removal and indoor air treatment: a review. *J. Phys. D: Appl. Phys.* 2014. V. 47. DOI: 10.1088/0022-3727/47/22/224011.
16. **Tu X., Christopher Whitehead J., Nozaki T.** Plasma Catalysis. Switzerland. Springer, Cham. 2019. DOI: 10.1007/978-3-030-05189-1.
17. **Van Durme J., Dewulf J., Leys C., Van Langenhove H.** Combining non-thermal plasma with heterogeneous catalysis in waste gas treatment: A review. *Appl. Catal.* 2008. V. 78. P. 324-333. DOI: 10.1016/j.apcatb.2007.09.035.
18. **Parmon V.N., Noskov A.S., Anfimova N.P., Shmachkova V.P.** The state and prospects of development of the catalyst sub-sector and catalysis developments in Russia. *Kataliz Promysh.* 2006. 1. P. 6-20 (in Russian).
19. **Gordina N.E., Prokof'ev V.Y., Hmylova O.E., Kul'pina Y.N.** Effect of ultrasound on the thermal behavior of the mixtures for the LTA zeolite synthesis based on metakaolin. *J. Therm. Anal.* 2017. V. 129. P. 1415-1427. DOI: 10.1007/s10973-017-6357-6.

20. Ильин А.А., Смирнов Н.Н., Румянцев Р.Н., Иванова Т.В., Ильин А.П. Механохимический синтез оксидов цинка с использованием жидких и газообразных сред. *Журн. прикл. химии*. 2014. Вып. 87. С. 1412-1416. DOI: 10.1134/S1070427214100036.
21. Baláz P. Mechanochemistry in Minerals Engineering. In: Mechanochemistry in Nanoscience and Minerals Engineering. Ed. by P. Baláz. Berlin, Heidelberg: Springer Berlin Heidelberg. 2008. P. 257-296. DOI: 10.1007/978-3-540-74855-7_5.
22. Zhao B., Chen Z., Yan X., Ma X., Hao Q. CO Methanation over Ni/SiO₂ Catalyst Prepared by Ammonia Impregnation and Plasma Decomposition. *Top Catal.* 2017. V. 60. P. 879-889. DOI: 10.1007/s11244-017-0752-x.
23. Butman M.F., Gushchin A.A., Ovchinnikov N.L., Gusev G.I., Zinenko N.V., Karamysheva S.P., Krämer K.W. Synergistic Effect of Dielectric Barrier Discharge Plasma and TiO₂-Pillared Montmorillonite on the Degradation of Rhodamine B in an Aqueous Solution. *Catalysts*. 2020. V. 10. P. 359. DOI: 10.3390/catal10040359.
24. Гусев Г.И., Гушин А.А., Гриневич В.И., Филиппов Д.В., Извекова Т.В. Физико-химические свойства сорбентов, применяемых для очистки сточных вод от нефтепродуктов. *Изв. вузов. Химия и химическая технология*. 2018. Т. 61. Вып. 7. С. 137-143. DOI: 10.6060/ivkkt.20186107.5686.
25. Мельников А.А., Гордина Н.Е., Тюканова К.А., Гусев Г.И., Гушин А.А., Румянцев Р.Н. Синтез сорбционных систем на основе механохимически активированного вермикулита. *Изв. вузов. Химия и хим. технология*. 2021. Т. 64. Вып. 8. С. 63-71. DOI: 10.6060/ivkkt.20216408.6422.
26. Hoseini S.N., Pirzaman A.K., Aroon M.A., Pirbazari A.E. Photocatalytic degradation of 2, 4-dichlorophenol by Co-doped TiO₂ (Co/TiO₂) nanoparticles and Co/TiO₂ containing mixed matrix membranes. *J. Water Process. Eng.* 2017. V. 17. P. 124-134. DOI: 10.1016/j.jwpe.2017.02.015.
27. Leong S., Razmjou A., Wang K., Hapgood K., Zhang X., Wang H. TiO₂ based photocatalytic membranes: A review. *J. Membr. Sci.* 2014. V. 472. P. 167-184. DOI: 10.1016/j.memsci.2014.08.016.
28. Hallaj T., Amjadi M. Determination of 2, 4-dichlorophenol in water samples using a chemiluminescence system consisting of graphene quantum dots, rhodamine B and cerium (IV) ion. *Mikrochim Acta*. 2016. V. 183. P. 1219-1225. DOI: 10.1007/s00604-016-1749-z.
29. Jiang G., Lan M., Zhang Z., Lv X., Lou Z., Xu X., Dong F., Zhang S. Identification of active hydrogen species on palladium nanoparticles for an enhanced electrocatalytic hydrodechlorination of 2, 4-dichlorophenol in water. *J. Environ. Sci. Technol.* 2017. V. 51. P. 7599-7605. DOI: 10.1021/acs.est.7b01128.
30. Wang Y., Zhang J.-X., Ren, H.-J., Wang, Y., Pan, H.-Y., Zhang, L.-Y. Phytoremediation potentiality of garlic roots for 2, 4-dichlorophenol removal from aqueous solutions. *Appl. Microbiol.* 2015. V. 99. P. 3629-3637. DOI: 10.1007/s00253-014-6277-3.
31. Xiao B., Cui L.-Q., Ding C., Wang H. Effects of lithium and 2, 4-dichlorophenol on zebrafish: circadian rhythm disorder and molecular effects. *Zebrafish*. 2017. V. 14. P. 209-215. DOI: 10.1089/zeb.2016.1389.
32. Angelini V.A., Agostini E., Medina M.I., González P.S. Use of hairy roots extracts for 2, 4-DCP removal and toxicity evaluation by *Lactuca sativa* test. *Environ. Sci. Pollut. Res.* 2014. V. 21. P. 2531-2539. DOI: 10.1007/s11356-013-2172-1.
20. P'in A.A., Smirnov N.N., Rumyantsev R.N., Ivanova T.V., P'in A.P., Mechanochemical synthesis of zinc oxides with the use of liquid and gaseous media. *Zhurn. Prikl. Khim.* 2014. 87. P. 1412-1416 (in Russian). DOI: 10.1134/S1070427214100036.
21. Baláz P. Mechanochemistry in Minerals Engineering. In: Mechanochemistry in Nanoscience and Minerals Engineering. Ed. by P. Baláz. Berlin, Heidelberg: Springer Berlin Heidelberg. 2008. P. 257-296. DOI: 10.1007/978-3-540-74855-7_5.
22. Zhao B., Chen Z., Yan X., Ma X., Hao Q. CO Methanation over Ni/SiO₂ Catalyst Prepared by Ammonia Impregnation and Plasma Decomposition. *Top Catal.* 2017. V. 60. P. 879-889. DOI: 10.1007/s11244-017-0752-x.
23. Butman M.F., Gushchin A.A., Ovchinnikov N.L., Gusev G.I., Zinenko N.V., Karamysheva S.P., Krämer K.W. Synergistic Effect of Dielectric Barrier Discharge Plasma and TiO₂-Pillared Montmorillonite on the Degradation of Rhodamine B in an Aqueous Solution. *Catalysts*. 2020. V. 10. P. 359. DOI: 10.3390/catal10040359.
24. Gusev G.I., Gushchin A.A., Grinevich V.I., Filippov D.V., Izvekova T.V. Physicochemical properties of sorbents used for wastewater treatment from oil products. *ChemChemTech [Izv. Vyssh. Uchebn. Zaved. Khim. Khim. Tekhnol.]*. 2018. V. 61. N 7. P. 137-143 (in Russian). DOI: 10.6060/ivkkt.20186107.5686.
25. Melnikov A.A., Gordina N.E., Tyukanova K.A., Gusev G.I., Gushchin A.A., Rumyantsev R.N. Synthesis of sorption systems based on mechanochemically activated vermiculite. *ChemChemTech [Izv. Vyssh. Uchebn. Zaved. Khim. Khim. Tekhnol.]*. 2021. V. 64. N 8. P. 63-71. DOI: 10.6060/ivkkt.20216408.6422.
26. Hoseini S.N., Pirzaman A.K., Aroon M.A., Pirbazari A.E. Photocatalytic degradation of 2, 4-dichlorophenol by Co-doped TiO₂ (Co/TiO₂) nanoparticles and Co/TiO₂ containing mixed matrix membranes. *J. Water Process. Eng.* 2017. V. 17. P. 124-134. DOI: 10.1016/j.jwpe.2017.02.015.
27. Leong S., Razmjou A., Wang K., Hapgood K., Zhang X., Wang H. TiO₂ based photocatalytic membranes: A review. *J. Membr. Sci.* 2014. V. 472. P. 167-184. DOI: 10.1016/j.memsci.2014.08.016.
28. Hallaj T., Amjadi M. Determination of 2, 4-dichlorophenol in water samples using a chemiluminescence system consisting of graphene quantum dots, rhodamine B and cerium (IV) ion. *Mikrochim Acta*. 2016. V. 183. P. 1219-1225. DOI: 10.1007/s00604-016-1749-z.
29. Jiang G., Lan M., Zhang Z., Lv X., Lou Z., Xu X., Dong F., Zhang S. Identification of active hydrogen species on palladium nanoparticles for an enhanced electrocatalytic hydrodechlorination of 2, 4-dichlorophenol in water. *J. Environ. Sci. Technol.* 2017. V. 51. P. 7599-7605. DOI: 10.1021/acs.est.7b01128.
30. Wang Y., Zhang J.-X., Ren, H.-J., Wang, Y., Pan, H.-Y., Zhang, L.-Y. Phytoremediation potentiality of garlic roots for 2, 4-dichlorophenol removal from aqueous solutions. *Appl. Microbiol.* 2015. V. 99. P. 3629-3637. DOI: 10.1007/s00253-014-6277-3.
31. Xiao B., Cui L.-Q., Ding C., Wang H. Effects of lithium and 2, 4-dichlorophenol on zebrafish: circadian rhythm disorder and molecular effects. *Zebrafish*. 2017. V. 14. P. 209-215. DOI: 10.1089/zeb.2016.1389.
32. Angelini V.A., Agostini E., Medina M.I., González P.S. Use of hairy roots extracts for 2, 4-DCP removal and toxicity evaluation by *Lactuca sativa* test. *Environ. Sci. Pollut. Res.* 2014. V. 21. P. 2531-2539. DOI: 10.1007/s11356-013-2172-1.

33. **Gu L., Chen Z., Sun C., Wei B., Yu X.** Photocatalytic degradation of 2, 4-dichlorophenol using granular activated carbon supported TiO₂. *Desalination*. 2010. V. 263. P. 107-112. DOI: 10.1016/j.desal.2010.06.045.
34. **Ormad M.P., Ovelleiro J.L., Kiwi J.** Photocatalytic degradation of concentrated solutions of 2,4-dichlorophenol using low energy light: Identification of intermediates. *Appl. Catal. B*. 2001. V. 32. P. 157-166. DOI: 10.1016/S0926-3373(01)00132-1.
35. **Buchanan I.D., Nicell J.A.** Model development for horseradish peroxidase catalyzed removal of aqueous phenol. *Biotechnol. Bioeng.* 1997. V. 54. P. 251-261. DOI: 10.1002/(sici)1097-0290(19970505)54:3%3C251::aid-bit6%3E3.0.co;2-e.
36. **Busca G., Berardinelli S., Resini C., Arrighi L.** Technologies for the removal of phenol from fluid streams: a short review of recent developments. *J. Hazard. Mater.* 2008. V. 160. P. 265-288. DOI: 10.1016/j.jhazmat.2008.03.045.
37. **Eapen S., Singh S., D'Souza S.F.** Advances in development of transgenic plants for remediation of xenobiotic pollutants. *Biotechnol. Adv.* 2007. V. 25. P. 442-451. DOI: 10.1016/j.biotechadv.2007.05.001.
38. **Heegn H.** On the connection between ultrafine grinding and mechanical activation of minerals. *Aufbereitungs-technik*. 1989. V. 30. P. 635-642.
39. **Delogu F., Deidda C., Mulas G., Schiffini L., Cocco G.** A quantitative approach to mechanochemical processes. *J. Mater. Sci.* 2004. V. 39. P. 5121-5124. DOI: 10.1023/B:JMSE.0000039194.07422.be.
40. **Gushchin A.A., Grinevich V.I., Gusev G.I., Kvitkova E.Y., Rybkin V.V.** Removal of Oil Products from Water Using a Combined Process of Sorption and Plasma Exposure to DBD. *Plasma Chem. Plasma*. 2018. V. 5. P. 1021-1033. DOI: 10.1007/s11090-018-9912-4.
41. **Гусев Г.И., Гушин А.А., Гринеvич В.И., Извекова Т.В., Квиткова Е.Ю., Рыбкин В.В.** Разрушение водных растворов 2,4-дихлорфенола в реакторе плазменно-каталитического барьерного разряда. *Изв. вузов. Химия и хим. технология*. 2021. Т. 64. Вып. 11. С. 103-111. DOI: 10.6060/ivkkt.20216411.6507.
42. Bird R.B., Stewart W.E., Lightfoot E.N. Transport phenomena. Wiley. 2006.
43. ГОСТ Р 51209-98. Вода питьевая. Способ определения содержания хлорорганических пестицидов методом газожидкостной хроматографии. Министерство здравоохранения России. 1998.
44. **Ekström T., Chatfield C., Wruss W., Maly-Schreiber M.** The use of X-ray diffraction peak-broadening analysis to characterize ground Al₂O₃ powders. *J. Mater. Sci.* 1985. V. 20. P. 1266-1274. DOI: 10.1007/BF01026322.
45. **Румянцев Р.Н., Мельников А.А., Батанов А.А., Проzorov Д.А., Ильин А.А., Афиневский А.В.** Влияние условий механохимической активации на физико-химические свойства оксида цинка. *Стекло и керамика*. 2020. Т. 93. № 10. С. 41-46.
46. **Huo X., Wu L., Liao L., Xia Z., Wang L.** The effect of interlayer cations on the expansion of vermiculite. *Powder Technol.* 2012. V. 224. P. 241-246. DOI: 10.1016/j.powtec.2012.02.059.
47. **Liu D., Deng S., Vakili M., Du R., Tao L., Sun J., Wang B., Huang J., Wang Y., Yu G.** Fast and high adsorption of Ni(II) on vermiculite-based nanoscale hydrated zirconium oxides. *Chem. Eng. Technol.* 2019. V. 360. P. 1150-1157. DOI: 10.1016/j.cej.2018.10.178.
33. **Gu L., Chen Z., Sun C., Wei B., Yu X.** Photocatalytic degradation of 2, 4-dichlorophenol using granular activated carbon supported TiO₂. *Desalination*. 2010. V. 263. P. 107-112. DOI: 10.1016/j.desal.2010.06.045.
34. **Ormad M.P., Ovelleiro J.L., Kiwi J.** Photocatalytic degradation of concentrated solutions of 2,4-dichlorophenol using low energy light: Identification of intermediates. *Appl. Catal. B*. 2001. V. 32. P. 157-166. DOI: 10.1016/S0926-3373(01)00132-1.
35. **Buchanan I.D., Nicell J.A.** Model development for horseradish peroxidase catalyzed removal of aqueous phenol. *Biotechnol. Bioeng.* 1997. V. 54. P. 251-261. DOI: 10.1002/(sici)1097-0290(19970505)54:3%3C251::aid-bit6%3E3.0.co;2-e.
36. **Busca G., Berardinelli S., Resini C., Arrighi L.** Technologies for the removal of phenol from fluid streams: a short review of recent developments. *J. Hazard. Mater.* 2008. V. 160. P. 265-288. DOI: 10.1016/j.jhazmat.2008.03.045.
37. **Eapen S., Singh S., D'Souza S.F.** Advances in development of transgenic plants for remediation of xenobiotic pollutants. *Biotechnol. Adv.* 2007. V. 25. P. 442-451. DOI: 10.1016/j.biotechadv.2007.05.001.
38. **Heegn H.** On the connection between ultrafine grinding and mechanical activation of minerals. *Aufbereitungs-technik*. 1989. V. 30. P. 635-642.
39. **Delogu F., Deidda C., Mulas G., Schiffini L., Cocco G.** A quantitative approach to mechanochemical processes. *J. Mater. Sci.* 2004. V. 39. P. 5121-5124. DOI: 10.1023/B:JMSE.0000039194.07422.be.
40. **Gushchin A.A., Grinevich V.I., Gusev G.I., Kvitkova E.Y., Rybkin V.V.** Removal of Oil Products from Water Using a Combined Process of Sorption and Plasma Exposure to DBD. *Plasma Chem. Plasma*. 2018. V. 5. P. 1021-1033. DOI: 10.1007/s11090-018-9912-4.
41. **Gusev G.I., Gushchin A.A., Grinevich V.I., Izveкова T.V., Kvitkova E.Y., Rybkin V.V.** Destruction of aqueous solutions of 2, 4-dichlorophenol in a plasma-catalytic barrier discharge reactor. *ChemChemTech [Izv. Vyssh. Uchebn. Zaved. Khim. Khim. Tekhnol.]*. 2021. V. 64. N 11. P. 103-111. DOI: 10.6060/ivkkt.20216411.6507.
42. Bird R.B., Stewart W.E., Lightfoot E.N. Transport phenomena. Wiley. 2006.
43. ГОСТ Р 51209-98, 1998. Drinking water. Method for determining the content of organochlorine pesticides by gas-liquid chromatography. Ministry of Health of Russia. 1998 (in Russian).
44. **Ekström T., Chatfield C., Wruss W., Maly-Schreiber M.** The use of X-ray diffraction peak-broadening analysis to characterize ground Al₂O₃ powders. *J. Mater. Sci.* 1985. V. 20. P. 1266-1274. DOI: 10.1007/BF01026322.
45. **Rumyantsev R.N., Melnikov A.A., Batanov A.A., Prozorov D.A., Il'in A.A., Afineevskij A.V.** Influence of the conditions of mechanochemical activation on the physical and chemical properties of zinc oxide. *Glass and ceramics*. 2020. V. 93. N 10. P. 41-46.
46. **Huo X., Wu L., Liao L., Xia Z., Wang L.** The effect of interlayer cations on the expansion of vermiculite. *Powder Technol.* 2012. V. 224. P. 241-246. DOI: 10.1016/j.powtec.2012.02.059.
47. **Liu D., Deng S., Vakili M., Du R., Tao L., Sun J., Wang B., Huang J., Wang Y., Yu G.** Fast and high adsorption of Ni(II) on vermiculite-based nanoscale hydrated zirconium oxides. *Chem. Eng. Technol.* 2019. V. 360. P. 1150-1157. DOI: 10.1016/j.cej.2018.10.178.

48. **Gopalan R., Chang C.H., Lin Y.S.** Thermal stability improvement on pore and phase structure of sol-gel derived zirconia. *J. Mater. Sci.* 1995. V. 30. P. 3075-3081. DOI: 10.1007/BF01209219.
49. **Mercera P.D.L., Van Ommen J.G., Doesburg E.B.M., Burggraaf A.J., Ross J.R.H.** Zirconia as a support for catalysts: Evolution of the texture and structure on calcination in air. *Appl. Catal.* 1990. V. 57. P. 127-148. DOI: 10.1016/S0166-9834(00)80728-9.
50. **Borik M., Gerasimov M., Lomonova E., Milovich F., Myzina V., Ryabochkina P., Sidorova N., Tabachkova N.** Mechanical properties and transformation hardening mechanism in yttria, ceria, neodymia and ytterbia co-doped zirconia based solid solutions. *Mater. Chem. Phys.* 2019. V. 232. P. 28-33. DOI: 10.1016/j.matchemphys.2019.04.047.
51. **Иванов А.В., Кустов Л.М.** Твердые суперкислоты на основе оксида циркония: природа активных центров и изомеризация алканов. *Рос. хим. журн.* 2000. Том XLIV. С. 21-52.
52. **Ruiz-Conde A., Ruiz-Amil A., Perez-Rodriguez J.L., Sánchez-Soto P.J.** Dehydration–rehydration in magnesium vermiculite: conversion from two–one and one–two water layer hydration states through the formation of interstratified phases. *J. Mater. Chem.* 1996. V. 6. P. 1557-1566. DOI: 10.1039/JM9960601557.
53. **Suzuki M., Wada N., Hines D.R., Whittingham M.S.** Hydration states and phase transitions in vermiculite intercalation compounds. *Phys. Rev. B.* 1987. V. 36. P. 2844-2851. DOI: 10.1103/PhysRevB.36.2844.
54. **Acosta E.J., Deng Y., White G.N., Dixon J.B., McInnes K.J., Senseman S.A., Frantzen A.S., Simanek E.E.** Dendritic Surfactants Show Evidence for Frustrated Intercalation: A New Organoclay Morphology. *Chem. Mater.* 2003. V. 15. P. 2903-2909. DOI: 10.1021/cm0302328.
55. **Huang C., Fan E., Xu H., Li M., Shao G., Wang H., Lu H., Zhang R.** Effect of particle size of vermiculite on the microstructure and photocatalytic performance of g-C₃N₄/vermiculite composite. *Solid State Sci.* 2021. V. 113. DOI: 10.1016/j.solidstatesciences.2021.106533.
56. **Luo X., Wang C., Wang L., Deng F., Luo S., Tu X., Au C.** Nanocomposites of graphene oxide-hydrated zirconium oxide for simultaneous removal of As(III) and As(V) from water. *Chem. Eng. J.* 2013. V. 220. P. 98-106. DOI: 10.1016/j.cej.2013.01.017.
57. **Sprynskyy M., Kowalkowski T., Tutu H., Cukrowska E.M., Buszewski B.** Adsorption performance of talc for uranium removal from aqueous solution. *Chem. Eng. J.* 2011. V. 171. P. 1185-1193. DOI: 10.1016/j.cej.2011.05.022.
58. **Khalfaoui M., Knani S., Hachicha M.A., Lamine A.B.** New theoretical expressions for the five adsorption type isotherms classified by BET based on statistical physics treatment. *J. Colloid Interface Sci.* 2003. V. 263. P. 350-356. DOI: 10.1016/S0021-9797(03)00139-5.
59. **Lee D.H., Song Y.-H., Kim K.-T., Jo S., Kang H.** Current state and perspectives of plasma applications for catalyst regeneration. *Catal. Today.* 2019. V. 337. P. 15-27. DOI: 10.1016/j.cattod.2019.04.071.
60. **Wang B., Xiong Y., Han Y., Hong J., Zhang Y., Li J., Jing F., Chu W.** Preparation of stable and highly active Ni/CeO₂ catalysts by glow discharge plasma technique for glycerol steam reforming. *Appl. Catal. B.* 2019. V. 249. P. 257-265. DOI: 10.1016/j.apcatb.2019.02.074.
48. **Gopalan R., Chang C.H., Lin Y.S.** Thermal stability improvement on pore and phase structure of sol-gel derived zirconia. *J. Mater. Sci.* 1995. V. 30. P. 3075-3081. DOI: 10.1007/BF01209219.
49. **Mercera P.D.L., Van Ommen J.G., Doesburg E.B.M., Burggraaf A.J., Ross J.R.H.** Zirconia as a support for catalysts: Evolution of the texture and structure on calcination in air. *Appl. Catal.* 1990. V. 57. P. 127-148. DOI: 10.1016/S0166-9834(00)80728-9.
50. **Borik M., Gerasimov M., Lomonova E., Milovich F., Myzina V., Ryabochkina P., Sidorova N., Tabachkova N.** Mechanical properties and transformation hardening mechanism in yttria, ceria, neodymia and ytterbia co-doped zirconia based solid solutions. *Mater. Chem. Phys.* 2019. V. 232. P. 28-33. DOI: 10.1016/j.matchemphys.2019.04.047.
51. **Ivanov A., Kustov L.** Solid superacids based on zirconium oxide: the nature of active centers and isomerization of alkanes. *Ros. Khim. Zhurn.* 2000. V. XLIV. P. 21-52 (in Russian).
52. **Ruiz-Conde A., Ruiz-Amil A., Perez-Rodriguez J.L., Sánchez-Soto P.J.** Dehydration–rehydration in magnesium vermiculite: conversion from two–one and one–two water layer hydration states through the formation of interstratified phases. *J. Mater. Chem.* 1996. V. 6. P. 1557-1566. DOI: 10.1039/JM9960601557.
53. **Suzuki M., Wada N., Hines D.R., Whittingham M.S.** Hydration states and phase transitions in vermiculite intercalation compounds. *Phys. Rev. B.* 1987. V. 36. P. 2844-2851. DOI: 10.1103/PhysRevB.36.2844.
54. **Acosta E.J., Deng Y., White G.N., Dixon J.B., McInnes K.J., Senseman S.A., Frantzen A.S., Simanek E.E.** Dendritic Surfactants Show Evidence for Frustrated Intercalation: A New Organoclay Morphology. *Chem. Mater.* 2003. V. 15. P. 2903-2909. DOI: 10.1021/cm0302328.
55. **Huang C., Fan E., Xu H., Li M., Shao G., Wang H., Lu H., Zhang R.** Effect of particle size of vermiculite on the microstructure and photocatalytic performance of g-C₃N₄/vermiculite composite. *Solid State Sci.* 2021. V. 113. DOI: 10.1016/j.solidstatesciences.2021.106533.
56. **Luo X., Wang C., Wang L., Deng F., Luo S., Tu X., Au C.** Nanocomposites of graphene oxide-hydrated zirconium oxide for simultaneous removal of As(III) and As(V) from water. *Chem. Eng. J.* 2013. V. 220. P. 98-106. DOI: 10.1016/j.cej.2013.01.017.
57. **Sprynskyy M., Kowalkowski T., Tutu H., Cukrowska E.M., Buszewski B.** Adsorption performance of talc for uranium removal from aqueous solution. *Chem. Eng. J.* 2011. V. 171. P. 1185-1193. DOI: 10.1016/j.cej.2011.05.022.
58. **Khalfaoui M., Knani S., Hachicha M.A., Lamine A.B.** New theoretical expressions for the five adsorption type isotherms classified by BET based on statistical physics treatment. *J. Colloid Interface Sci.* 2003. V. 263. P. 350-356. DOI: 10.1016/S0021-9797(03)00139-5.
59. **Lee D.H., Song Y.-H., Kim K.-T., Jo S., Kang H.** Current state and perspectives of plasma applications for catalyst regeneration. *Catal. Today.* 2019. V. 337. P. 15-27. DOI: 10.1016/j.cattod.2019.04.071.
60. **Wang B., Xiong Y., Han Y., Hong J., Zhang Y., Li J., Jing F., Chu W.** Preparation of stable and highly active Ni/CeO₂ catalysts by glow discharge plasma technique for glycerol steam reforming. *Appl. Catal. B.* 2019. V. 249. P. 257-265. DOI: 10.1016/j.apcatb.2019.02.074.

Поступила в редакцию (Received) 10.01.2022
Принята к публикации (Accepted) 16.03.2022